

OVERLAPPING DOMAIN DECOMPOSITION PRECONDITIONER FOR INTEGRAL EQUATIONS

CHAO CHEN* AND GEORGE BIROS†

Abstract. The discretization of certain integral equations, e.g., the first-kind Fredholm equation of Laplace’s equation, leads to symmetric positive-definite linear systems, where the coefficient matrix is dense and often ill-conditioned. We introduce a new preconditioner based on a novel overlapping domain decomposition that can be combined efficiently with fast direct solvers. Empirically, we observe that the condition number of the preconditioned system is $\mathcal{O}(1)$, independent of the problem size. Our domain decomposition is designed so that we can construct approximate factorizations of the subproblems efficiently. In particular, we apply the recursive skeletonization algorithm to subproblems associated with every subdomain. We present numerical results on problem sizes up to 16384^2 in 2D and 256^3 in 3D, which were solved in less than 16 hours and three hours, respectively, on an Intel Xeon Platinum 8280M.

Key words. Integral Equations, Overlapping Domain Decomposition, Symmetric Positive-definite Preconditioners, Fast Direct Solvers, Hierarchical Matrices

AMS subject classifications. 35R09, 65F08, 65N55,

1. Introduction. Consider the following integral equation (IE)

$$(1.1) \quad a(x)u(x) + b(x) \int_{\Omega} K(x-y)c(y)u(y)dy = f(x), \quad x \in \Omega \subset \mathbb{R}^d,$$

where $d = 2$ or 3 , $a(x), b(x), c(x)$ and $f(x)$ are given functions, $K(r) \equiv K(x-y)$ is the Green’s function of an elliptic operator, Ω is a finite simply-connected domain, and $u(x)$ is the unknown. Upon discretization of (1.1) through either Galerkin or Nyström methods, we obtain

$$(1.2) \quad A u = f,$$

where u and f are the discrete analogues of $u(x)$ and $f(x)$, respectively, and $A \in \mathbb{R}^{N \times N}$ is a *dense* matrix. See an example of the discretization in Section 2.

We further assume the discretized integral operator, A in (1.2), is symmetric positive-definite (SPD). This typically occurs when (1.1) is a first-kind Fredholm integral equation for Laplace’s equation or the Stokes equation, which has applications in magnetostatics, electrostatics and fluid dynamics. More theory and discussion on symmetric formulations of integral equations (including hypersingular integrals) can be found in [25]. One challenge for solving (1.2) is that A usually has a large condition number [37,38], and this paper is concerned with solving (1.2) iteratively using domain decomposition preconditioners.

1.1. Previous work. Since A is a dense matrix, classical direct methods such as Gaussian elimination require $\mathcal{O}(N^3)$ operations and $\mathcal{O}(N^2)$ storage. Such costs limit the application of these methods to solving only small problems.

Although A is a dense matrix, in many applications it is *data sparse* in the sense that the singular values of certain off-diagonal blocks in A decay exponentially fast. This is typically the case for matrices related to integral equation formulations of problems with non-oscillatory coefficients and kernels. The numerical low-rank property is exploited in the fast multipole method (FMM) [7,13,16,20,23,39], which requires only

*University of Texas at Austin, United States (chenchao.nk@gmail.com,biros@oden.utexas.edu).

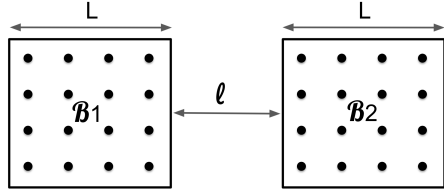


Fig. 1: Given two sets of points \mathcal{B}_1 and \mathcal{B}_2 inside two boxes, respectively. If the two boxes are adjacent (weak admissibility), i.e., $\ell = 0$, then the numerical rank of the off-diagonal block $A(\mathcal{B}_1, \mathcal{B}_2)$ is $\mathcal{O}(L)$. On the other hand, if the two boxes are well-separated (strong admissibility), i.e., $\ell = \mathcal{O}(L)$, then the numerical rank of the off-diagonal block $A(\mathcal{B}_1, \mathcal{B}_2)$ is $\mathcal{O}(1)$.

$\mathcal{O}(N)$ operations and storage for applying A to a vector. Such a fast matrix-vector multiplication can be coupled with iterative methods such as the conjugate gradient method [29] to solve (1.2). However, the number of iterations can be large when the condition number of A is large. Such a situation occurs when (1.1) is a first-kind Fredholm integral equation; when $a(x)$, $b(x)$ or $c(x)$ exhibit high contrast; or when the problem domain has a complex geometry.

To accelerate the convergence of an iterative method for solving (1.2), the block Jacobi preconditioner is arguably the simplest preconditioner but may not be particularly effective. It was observed empirically that the single-level additive Schwarz preconditioner with overlapping blocks led to better convergence for some realistic engineering applications [26, 27]. Previous work on two-level additive Schwarz preconditioners mainly focused on analyzing the condition number of the preconditioned linear system. In [31] and [25], the authors introduced two-level additive Schwarz preconditioners to solve first-kind boundary integral equations for the Laplace's equation on a curve in \mathbb{R}^2 and on an open surface in \mathbb{R}^3 , respectively. In [31], overlapping domain decomposition was used, and it was proved that the condition number of the preconditioned linear system is bounded only if the coarse mesh size is proportional to the size of overlap. In [25], non-overlapping domain decomposition was used, and it was proved that the condition number of the preconditioned linear system still depends on the ratio between the sizes of the coarse mesh and the fine mesh. Recently, the authors of [3] introduced a two-level additive Schwarz preconditioner based on overlapping domain decomposition, which showed great potential in solving *indefinite* dense linear systems from the discretization of the Lippmann-Schwinger equation. For a more detailed discussion on existing preconditioners for solving discretized integral equations, we refer interested readers to [28] and the references therein.

Fast direct solvers (FDS's) are a class of methods that construct approximate factorizations with a tunable accuracy. When the accuracy is low, they can be used as preconditioners; otherwise with a high accuracy, they behave similarly as a direct method that is suitable for solving multiple right-hand sides. The basic idea of an FDS is to compress certain off-diagonal blocks in A to a prescribed accuracy because they are numerically low rank. This class of methods can be further divided into two groups based on which off-diagonal blocks are compressed or the admissibility criteria; see Figure 1.

The first group employs the so-called weak admissibility and compresses off-diagonal blocks corresponding to two spatially adjacent regions. The resulting nu-

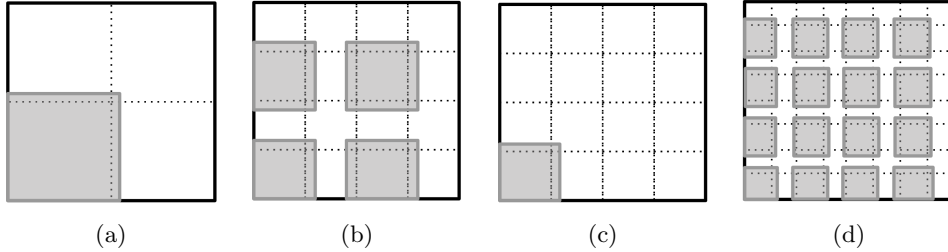


Fig. 2: A subdomain (grey) in the Schwarz or the CBD preconditioner. Dashed lines indicate the partitioning $\Omega = \bigcup_{i=1}^M \mathcal{P}_i$, and every box in grey stands for an extended partition $\tilde{\mathcal{P}}_i$. (a) Schwarz preconditioner with four subdomains. (b) CBD preconditioner with four subdomains, where every subdomain has four separated regions. (c) Schwarz preconditioner with 16 subdomains. (d) CBD preconditioner with four subdomains, where every subdomain has 16 separated regions.

numerical ranks typically increase proportionally to the perimeter or the surface area of the regions in 2D or 3D, respectively. Consequently, the construction time of these methods typically scale as $\mathcal{O}(N^{3/2})$ and $\mathcal{O}(N^2)$ in 2D and 3D, respectively [1, 5, 6, 14, 15, 18, 22, 34, 36]. Assuming the same rank behavior on the Schur complement, this type of methods can be further accelerated to attain quasilinear complexity [10, 19, 35]. But existing numerical results seem to indicate that reaching the asymptotic regime requires a really large problem size in 3D.

The second group employs the so-called strong admissibility and compresses off-diagonal blocks corresponding to two sufficiently distant regions [11, 24, 30]. The resulting numerical ranks are constant regardless of the sizes of the regions according to standard fast multipole estimates [16, 17]. Consequently, these methods can achieve quasilinear complexity assuming the constant-rank estimates also hold for the Schur complement, which appears to be true in practice but lacks firm theoretical support. In practice, the constants in the asymptotic scalings tend to be quite large, especially in 3D, because off-diagonal blocks corresponding to adjacent regions are treated exactly without compression.

1.2. Contributions. We introduce a new preconditioner based on overlapping domain decomposition to solve (1.2) iteratively with the preconditioned conjugate gradient (PCG) method. The key feature is that the number of iterations required is $\mathcal{O}(1)$, independent of the problem size. Our method is based on an empirically observation of the single-level additive-Schwarz preconditioner (Schwarz preconditioner T_{Schwarz}^{-1} hereafter): the minimum eigenvalue of the preconditioned matrix is lower bounded away from zero. In other words, there exists a positive constant $C > 0$ such that $\lambda_{\min}(T_{\text{Schwarz}}^{-1} A) \geq C$. Our preconditioner is associated with a new strategy for constructing an overlapping domain decomposition that has a fixed number of subdomains, and we apply an FDS as a subdomain solver to construct the preconditioner efficiently. In the following, we illustrate these ideas in more details.

Let a partitioning (non-overlapping decomposition) of the problem domain be $\Omega = \bigcup_{i=1}^M \mathcal{P}_i$, where $\mathcal{P}_i \cap \mathcal{P}_j = \emptyset$ if $i \neq j$, and $M = \mathcal{O}(N)$. An overlapping decomposition $\Omega = \bigcup_{i=1}^M \tilde{\mathcal{P}}_i$ is obtained by extending \mathcal{P}_i to overlap with its neighbors, so that $\mathcal{P}_i \subset$

$\tilde{\mathcal{P}}_i$ and $\mathcal{P}_j \cap \tilde{\mathcal{P}}_i \neq \emptyset$ if \mathcal{P}_i and \mathcal{P}_j are spatially adjacent. See [Figures 2a](#) and [2c](#) for two examples of the domain decomposition corresponding to $M = 4$ and 16 , respectively. In the Schwarz preconditioner, every $\tilde{\mathcal{P}}_i$ is a subdomain, and we solve M corresponding subproblems, which are diagonal sub-blocks in A (up to a permutation). The Schwarz preconditioner T_{Schwarz}^{-1} can be viewed as a generalization of the block Jacobi preconditioner T_{Jacobi}^{-1} , where a subproblem is associated with \mathcal{P}_i rather than $\tilde{\mathcal{P}}_i$. Numerical results show that $\lambda_{\min}(T_{\text{Schwarz}}^{-1}A) \geq C > 0$, whereas $\lambda_{\min}(T_{\text{Jacobi}}^{-1}A)$ decreases toward zero as $N \rightarrow \infty$.

The new overlapping domain decomposition that we introduce is a coloring-based decomposition (CBD). The key feature of the CBD is that the number of subdomains is fixed, and every subdomain Ω_i consists of spatially distant $\tilde{\mathcal{P}}_i$'s. See [Figures 2b](#) and [2d](#) for two examples of a subdomain in the CBD corresponding to $M = 16$ and 64 , respectively. To compute such a decomposition, we apply graph coloring to the adjacency graph of $\{\mathcal{P}_i\}_{i=1}^M$, so every \mathcal{P}_i (and $\tilde{\mathcal{P}}_i$) is assigned a color c_i . Then, a subdomain Ω_i consists of \mathcal{P}_k 's of the same color, i.e., $\Omega_i = \bigcup_{c_k=i} \tilde{\mathcal{P}}_k$. Given a CBD, we define the corresponding preconditioner (CBD preconditioner hereafter) T_{CBD}^{-1} following the same algebraic formulation of the Schwarz preconditioner except that a subproblem A_i is associated with a subdomain Ω_i instead of a single $\tilde{\mathcal{P}}_i$. As a result, the diagonal blocks in A_i (with an appropriate permutation) are the subproblems in a related Schwarz preconditioner. In other words, the CBD preconditioner incorporates more information (off-diagonal blocks) from the global problem A . So we expect T_{CBD}^{-1} to be a better preconditioner than T_{Schwarz}^{-1} and thus $\lambda_{\min}(T_{\text{CBD}}^{-1}A) \geq \lambda_{\min}(T_{\text{Schwarz}}^{-1}A) \geq C > 0$. Under mild assumptions, the number of subdomains is upper bounded. For example, we have at most four subdomains in 2D and eight subdomains for a uniform partitioning in 3D. This implies that the maximum eigenvalue of the preconditioned matrix is upper bounded. Therefore, the condition number of $T_{\text{CBD}}^{-1}A$ is bounded; consequently, [\(1.2\)](#) can be solved in $\mathcal{O}(1)$ PCG iterations.

To accelerate the construction and reduce the memory footprint of the CBD preconditioner, we apply an FDS to A_i associated with every subdomain Ω_i . For demonstration, we employ the recursive skeletonization (RS) factorization [\[19\]](#) based on weak admissibility. RS has a relatively simple formulation, and its theoretical complexity is well understood (without any rank assumptions on the Schur complement). If the RS is applied to the global problem A directly, the problem domain Ω is partitioned at multiple scales, and then the interaction between every pair of adjacent regions is compressed recursively down to the leaf (finest) level. At the leaf level, we have $\Omega = \bigcup_{i=1}^M \mathcal{P}_i$, where the interaction rank is proportional to the perimeter or the surface area of every \mathcal{P}_i in 2D or 3D, respectively. This type of rank estimation also holds for coarse partitioning.

Consider a subdomain $\Omega_i = \bigcup_{c_k=i} \tilde{\mathcal{P}}_k$ in the CBD preconditioner, which consists of distant regions at the leaf level. When we apply RS to A_i associated with Ω_i , the separation distance among regions leads to significantly smaller number of skeletons at all scales, compared to the case when these regions are adjacent. In particular, the interaction rank between every pair of regions at the leaf level is provably constant (as in the FMM) because they satisfy the strong admissibility condition. As a result, the construction cost of the CBD preconditioner is much smaller than that of applying the RS to A directly.

Finally, we clarify that it is not as efficient as the CBD preconditioner if we fix the number of subdomains in the Schwarz preconditioner (problem size per subdo-

main increases as $\mathcal{O}(N)$) and employ the RS as the subdomain solver. The reason is basically the same as above that the interaction rank between a pair of adjacent regions is larger than that between a pair of distant regions. So the cost associated with every subdomain is larger than that in the CBD preconditioner. See more details in [Remark 4.8](#).

1.3. Outline and notations. In [Section 2](#), we introduce a model problem and overlapping domain decompositions that we use throughout this paper. In [Section 3](#), we define the Schwarz preconditioner T_{Schwarz}^{-1} and show the crucial observation that $\lambda_{\min}(T_{\text{Schwarz}}^{-1}A) \geq C > 0$. In [Section 4](#), we introduce the CBD preconditioner T_{CBD}^{-1} , show results on the spectrum of $T_{\text{CBD}}^{-1}A$, and discuss using the RS to construct T_{CBD}^{-1} efficiently. In [Section 5](#), we present numerical results to demonstrate the performance of the CBD preconditioner, and [Section 6](#) draws conclusions.

We adopt the MATLAB notation of submatrices, e.g., $A(\mathcal{I}, :)$ and $A(:, \mathcal{I})$ denote the rows and columns in matrix A corresponding to an index set \mathcal{I} , respectively.

2. Model problem and domain decomposition. In this section, we introduce a model problem and the discretized linear system to be solved. We also present two strategies for constructing an overlapping domain decomposition $\Omega = \bigcup_{i=1}^D \Omega_i$, where $\Omega \subset \mathbb{R}^d$ is the problem domain ($d = 2$ or 3), Ω_i 's are overlapping subdomains, and D is the number of subdomains.

For illustration purpose, we assume $\Omega = [0, 1]^d$, a uniform discretization grid of size $N = n^d$, and a uniform partitioning of the grid with $M = m^d$ partitions, where n and m are the number of grid points and partitions per dimension, respectively. So every partition has $N/M = (n/m)^d$ grid points. In this paper, we always assume $M = \mathcal{O}(N)$ unless stated otherwise. In [Section 2.2](#), we introduce the overlapping domain decomposition for the Schwarz preconditioner, where the number of subdomains equals the number of partitions, i.e., $D = M$. In [Section 2.3](#), we introduce the CBD strategy, where the number of subdomains $D = 2^d$. These setups are used throughout this paper for numerical results.

2.1. IE for Laplace's equation. We focus on a prototypical example of [\(1.1\)](#), the first-kind volume IE of Laplace's equation in 2D and 3D:

$$(2.1) \quad \int_{\Omega} K(x - y) u(y) dy = f(x), \quad x \in \Omega = [0, 1]^d,$$

where $K(r) \equiv K(x - y)$ is the fundamental solution of the free-space Laplace's equation, i.e.,

$$(2.2) \quad K(r) = \begin{cases} -\frac{1}{2\pi} \log(\|r\|), & d = 2, \\ \frac{1}{4\pi\|r\|}, & d = 3. \end{cases}$$

Here $u(x)$ is a scalar, and the extension of our approach to cases where $u(x)$ is a vector (e.g., in the Stokes equation) is straightforward.

For simplicity, we discretize [\(2.1\)](#) with a piecewise-constant collocation method over a uniform grid as follows. In 2D, let $h = 1/n$ and $x_j = h(j_1 - 1/2, j_2 - 1/2)$, where j is the index for an integer pair (j_1, j_2) for $1 \leq j_1, j_2 \leq n$. Using the trapezoidal rule and all x_j 's as the collocation points, [\(2.1\)](#) is discretized into the following linear system

$$(2.3) \quad \sum_j A_{ij} u_j = f_i$$

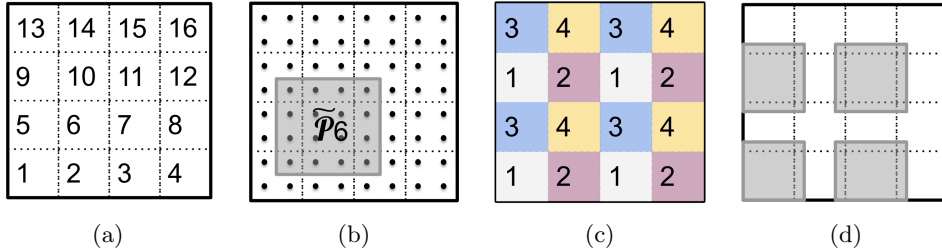


Fig. 3: (a) A uniform partitioning of the unit square $\Omega = \bigcup_{i=1}^{16} \mathcal{P}_i$. (b) A uniform grid with 8^2 points and an extended partition $\tilde{\mathcal{P}}_6$ (shaded) containing 4^2 points. (c) A four-coloring of the partitioning. (d) A subdomain Ω_1 (shaded) with four spatially separated regions in CBD.

where $u_j \approx u(x_j)$ is to be solved, $f_i = f(x_i)$ is given, and

$$(2.4) \quad A_{ij} = \begin{cases} h^2 K(x_i - x_j), & i \neq j, \\ \int_{-h/2}^{h/2} \int_{-h/2}^{h/2} K(r) dx dy, & i = j, \end{cases}$$

can be evaluated using (2.2) and a proper singular quadrature.

In 3D, let $h = 1/n$ and $x_j = h(j_1 - 1/2, j_2 - 1/2, j_3 - 1/2)$, where j is the index for an integer pair (j_1, j_2, j_3) for $1 \leq j_1, j_2, j_3 \leq n$. The same procedure as above leads to

$$(2.5) \quad A_{ij} = \begin{cases} h^3 K(x_i - x_j), & i \neq j, \\ \int_{-h/2}^{h/2} \int_{-h/2}^{h/2} \int_{-h/2}^{h/2} K(r) dx dy dz, & i = j. \end{cases}$$

2.2. Overlapping domain decomposition. Let a uniform partitioning or non-overlapping domain decomposition of the problem domain $\Omega = [0, 1]^d$ be

$$(2.6) \quad \Omega = \bigcup_{i=1}^M \mathcal{P}_i,$$

where $M = \mathcal{O}(N)$, and $\mathcal{P}_i \cap \mathcal{P}_j = \emptyset$ if $i \neq j$; see Figure 3a for an example. An overlapping domain decomposition $\Omega = \bigcup_{i=1}^M \tilde{\mathcal{P}}_i$, follows by extending \mathcal{P}_i to overlap with all of its spatially adjacent partitions \mathcal{P}_j , i.e., $\mathcal{P}_i \subset \tilde{\mathcal{P}}_i$ and $\mathcal{P}_j \cap \tilde{\mathcal{P}}_i \neq \emptyset$. In particular, we extend every partition \mathcal{P}_i to include one extra layer of grids in every direction (when possible) to form $\tilde{\mathcal{P}}_i$; see Figure 3b for an example. Except for those extended partitions near the boundary, every $\tilde{\mathcal{P}}_i$ has $(n/m+2)^d$ nodes given a uniform partitioning of a uniform grid.

Our first overlapping domain decomposition is simply taking $\Omega_i = \tilde{\mathcal{P}}_i$ as a subdomain. Hence, we get

$$(2.7) \quad \Omega = \bigcup_{i=1}^M \tilde{\mathcal{P}}_i = \bigcup_{i=1}^D \Omega_i,$$

where $D = M = \mathcal{O}(N)$ is the number of subdomains. In Section 3, (2.7) and (2.6) are used to construct the Schwarz preconditioner and the block Jacobi preconditioner, respectively. In the block Jacobi preconditioner, \mathcal{P}_i is treated as a subdomain.

Table 1: Given a domain decomposition $\Omega = \bigcup_{i=1}^D \Omega_i$, the definition of a subdomain Ω_i leads to different preconditioners including the block Jacobi preconditioner (Section 3), the Schwarz preconditioner (Section 3), and the CBD preconditioner (Section 4).

	Jacobi	Schwarz	CBD
Ω_i	\mathcal{P}_i	$\tilde{\mathcal{P}}_i$	$\bigcup_{c_k=i} \tilde{\mathcal{P}}_k$

2.3. Coloring-based decomposition. Given the partitioning in (2.6), we apply graph coloring to the adjacency graph of $\{\mathcal{P}_i\}_{i=1}^M$, where an edge between \mathcal{P}_i and \mathcal{P}_j exists if the two partitions are spatially adjacent. As a result, every partition \mathcal{P}_i (and its extension $\tilde{\mathcal{P}}_i$) is assigned a color c_i in $\{1, 2, \dots, N_c\}$, where N_c is the number of colors; see Figure 3c for an example. With the overlapping domain decomposition in (2.7), we form a subdomain Ω_i as

$$(2.8) \quad \Omega_i = \bigcup_{c_k=i} \tilde{\mathcal{P}}_k, \quad i = 1, 2, \dots, N_c;$$

see Figure 3d for an example. It is easy to see

$$(2.9) \quad \Omega = \bigcup_{i=1}^M \tilde{\mathcal{P}}_i = \bigcup_{i=1}^{N_c} \left(\bigcup_{c_k=i} \tilde{\mathcal{P}}_k \right) = \bigcup_{i=1}^D \Omega_i,$$

where $D = N_c$ is the number of subdomains. We call (2.9) a coloring-based decomposition (CBD), which is used in Section 4 to construct the CBD preconditioner. If the number of partitions $M = 2^d$ in (2.6), then (2.9) reduces to (2.7) because every subdomain (color) has only one partition.

According to the four color theorem [2], we know $N_c = 4$ in 2D. For a general graph in 3D, N_c can be arbitrarily large but is usually small for practical problems that have some regularity. For example, $N_c = 8$ for a uniform partitioning of a uniform grid. To summarize, we state the following:

THEOREM 2.1. *For a uniform partitioning of a uniform grid over $\Omega = [0, 1]^d$, the number of subdomains (colors) is 2^d in the CBD.*

As a summary of Sections 2.2 and 2.3, Table 1 shows the three preconditioners to be introduced associated with (2.6), (2.7), and (2.9).

3. Schwarz preconditioner. Given a domain decomposition $\Omega = \bigcup_{i=1}^D \Omega_i$ (not necessarily an overlapping domain decomposition), we construct a preconditioner as follows. Let \mathcal{I}_i denote the indices of the discretization points in Ω_i . First, we define the restriction operator for every subdomain Ω_i :

$$R_i = I_N(\mathcal{I}_i, :),$$

a subset of rows in the identity matrix $I_N \in \mathbb{R}^{N \times N}$ corresponding to indices \mathcal{I}_i . Then, we define the subproblem associated with Ω_i :

$$(3.1) \quad A_i = R_i A R_i^\top.$$

Finally, we define the preconditioner:

$$(3.2) \quad T^{-1} = \sum_{i=1}^D R_i^\top A_i^{-1} R_i.$$

With the overlapping domain decompositions (2.7) and (2.9), we obtain the Schwarz preconditioner (technically, single-level additive Schwarz preconditioner) and the CBD preconditioner (Section 4). With the non-overlapping domain decomposition (2.6), we obtain the block Jacobi preconditioner.

In the following, we focus on the Schwarz preconditioner T_{Schwarz}^{-1} , derive a theorem on $\lambda_{\max}(T_{\text{Schwarz}}^{-1}A)$, and show empirical results on $\lambda_{\min}(T_{\text{Schwarz}}^{-1}A)$. We also compare the Schwarz preconditioner to the block Jacobi preconditioner.

3.1. Maximum and minimum eigenvalues. Consider the preconditioned matrix

$$(3.3) \quad T^{-1}A = \sum_{i=1}^D R_i^\top A_i^{-1} R_i A.$$

We define

$$(3.4) \quad P_i = R_i^\top A_i^{-1} R_i A,$$

and we can verify that P_i is an orthogonal projection with respect to the inner product defined by the SPD matrix A :

$$P_i^2 = P_i, \quad AP_i = P_i^\top A.$$

As a result, we have

$$\lambda_{\max}(P_i) = 1,$$

which immediately leads to the following:

THEOREM 3.1. *Let A be an SPD matrix and the preconditioner T^{-1} defined in (3.2). Then,*

$$\lambda_{\max}(T^{-1}A) \leq D,$$

where D is the number of subdomains.

Proof. $\lambda_{\max}(T^{-1}A) \leq \sum_{i=1}^D \lambda_{\max}(P_i) = D$. \square

Note the theorem applies to both the block Jacobi and the Schwarz preconditioners because it only requires a decomposition of the problem domain (not necessarily an overlapping decomposition); see numerical results in Table 2. The table also shows that as the problem size N increases, $\lambda_{\min}(T_{\text{Schwarz}}^{-1}A)$ appears to converge to a positive constant close to one, whereas $\lambda_{\min}(T_{\text{Jacobi}}^{-1}A)$ is much smaller and keeps decreasing. We state the following (and provide more concrete evidence in Section 3.2):

Conjecture 3.2. Let A be the discretized integral operator in (2.4) or (2.5). Given the overlapping domain decomposition (2.7), the Schwarz preconditioner T_{Schwarz}^{-1} is defined in (3.2). Then,

$$\lambda_{\min}(T_{\text{Schwarz}}^{-1}A) \geq C > 0,$$

where C is a positive constant.

Remark 3.3. If A is a sparse SPD matrix arising from a local discretization (e.g., by finite elements or finite differences) of a second-order self-adjoint, coercive elliptic problem, then the upper bound in Theorem 3.1 can be reduced to a constant, independent of the number of subdomains D [4, 12]. The reason is that $P_i + P_j$ is still an orthogonal projection when $\Omega_i \cap \Omega_j = \emptyset$ ($R_i A R_j^\top = 0$ when A is sparse).

Table 2: Maximum and minimum eigenvalues of the preconditioned matrix (3.3). The block Jacobi and the Schwarz preconditioners are defined in Table 1. The number of subdomains $D = \mathcal{O}(N)$.

N	D	Jacobi		Schwarz	
		λ_{\max}	λ_{\min}	λ_{\max}	λ_{\min}
8^2	2^2	2.8479	0.1695	4.0000	0.8209
16^2	4^2	6.6883	0.0804	8.8046	0.9112
32^2	8^2	19.3756	0.0533	23.5948	0.9350
64^2	16^2	61.6629	0.0409	71.5192	0.9360
128^2	32^2	205.7705	0.0336	231.7813	0.9331

(a) Discretized integral operator in 2D; see (2.4).

N	D	Jacobi		Schwarz	
		λ_{\max}	λ_{\min}	λ_{\max}	λ_{\min}
4^3	2^3	4.0618	0.2602	8.0000	0.9750
8^3	4^3	15.4234	0.2056	33.1198	0.9942
16^3	8^3	60.9327	0.1916	134.7002	0.9967
32^3	16^3	242.9799	0.1878	547.3752	0.9972

(b) Discretized integral operator in 3D; see (2.5).

Remark 3.4. In the context of solving PDEs, the (single-level additive) Schwarz preconditioner results in a bounded maximum eigenvalue of the preconditioned matrix, whereas the minimum eigenvalue goes to zero as $M = \mathcal{O}(N) \rightarrow \infty$. Interestingly, the observation for solving IEs considered in this paper is reversed.

3.2. Analysis for $D = 2^d$. In this section, we assume the number of subdomains $D = 2^d$ and study the maximum and minimum eigen-pairs of $T_{\text{Schwarz}}^{-1}A$. The analysis of the maximum eigen-pair prepares for the corresponding analysis for $T_{\text{CBD}}^{-1}A$ in subsection 4.1. The observations for the minimum eigen-pair provide insights and evidence for Conjecture 3.2. We also compare the Schwarz preconditioner to the block Jacobi preconditioner, for which Conjecture 3.2 does not hold. Recall P_i defined in (3.4) is a projection associated with subdomain Ω_i , so we have

LEMMA 3.5. *Let $x \in \mathbb{R}^N$ be nonzero only in Ω_i , i.e., $x = R_i^\top R_i x$. Then,*

$$P_i x = x.$$

Proof. With the definitions of A_i and P_i in (3.1) and (3.4), respectively, we have

$$P_i x = (R_i^\top A_i^{-1} R_i A)(R_i^\top R_i x) = R_i^\top A_i^{-1} (R_i A R_i^\top) R_i x = R_i^\top R_i x = x. \quad \square$$

The lemma is useful for analyzing eigenvectors of the preconditioned matrix. The following theorem addresses the maximum eigenvalue and the associated eigenvector of $T_{\text{Schwarz}}^{-1}A$.

THEOREM 3.6. *Suppose the problem domain $\Omega = [0, 1]^d$ is partitioned uniformly into $D = 2^d$ overlapping subdomains. Given the overlapping domain decomposition*



Fig. 4: (a) $D = 4$ in (2.7). Shaded regions are shared by adjacent subdomains, and the four grid points at the center are shared by all four subdomains. (b) $D = 4$ in (2.6). As $N \rightarrow \infty$, all four subdomains contain the center of the square.

(2.7), we have

$$\lambda_{\max}(T_{\text{Schwarz}}^{-1} A) = 2^d,$$

and the corresponding eigen-space is of dimension 2^d and consists of vectors that are nonzero only in the overlapped region shared by all 2^d subdomains.

Proof. According to [Theorem 3.1](#), we know that $\lambda_{\max}(T_{\text{Schwarz}}^{-1} A) \leq 2^d$. Recall that when $D = 2^d$, we have $\cap_{i=1}^{2^d} \Omega_i \neq \emptyset$, and the shared region contains 2^d grid points; see [Figure 4a](#) for an example. Suppose x is nonzero only in the shared region. According to [Lemma 3.5](#), we know that $P_i x = x$ for all i . Therefore,

$$T_{\text{Schwarz}}^{-1} A x = \sum_{i=1}^{2^d} P_i x = 2^d x. \quad \square$$

The theorem does not apply to $T_{\text{Jacobi}}^{-1} A$ directly but provides insight on the maximum eigen-pair when the problem size $N \rightarrow \infty$. In the limit, all subdomains associated with the block Jacobi preconditioner share the center of the problem domain $\Omega = [0, 1]^d$; see [Figure 4b](#) for an example. So we know that

$$(3.5) \quad \lim_{N \rightarrow \infty} \lambda_{\max}(T_{\text{Jacobi}}^{-1} A) = 2^d;$$

see numerical results in [Table 3](#). The corresponding eigenvector converges to the indicator function of the center point x_c , i.e.,

$$(3.6) \quad \mathbf{1}_{x_c}(x) = \begin{cases} 1 & x = x_c, \\ 0 & \text{else}; \end{cases}$$

see numerical results plotted in [Figures 5a](#) and [5c](#).

Next, we consider the minimum eigen-pair of $T_{\text{Jacobi}}^{-1} A$. We start with an example in one dimension (1D). Suppose the problem domain $\Omega = [0, 1]$ is cut into two halves of equal length ($D = 2$), i.e., $\Omega_1 = [0, 1/2]$, $\Omega_2 = [1/2, 1]$. Suppose a uniform discretization grid has N nodes, where N is an even integer and the discretization points are indexed from left to right. Let the indices of discretization points in Ω_1 and Ω_2 be $\mathcal{I}_1 = \{1, 2, \dots, N/2\}$ and $\mathcal{I}_2 = \{N/2 + 1, N/2 + 2, \dots, N\}$, respectively. Recall the block Jacobi preconditioner T_{Jacobi}^{-1} defined in [\(3.2\)](#). Consider the eigenvalue problem

$$(3.7) \quad T_{\text{Jacobi}}^{-1} A x = \lambda x,$$

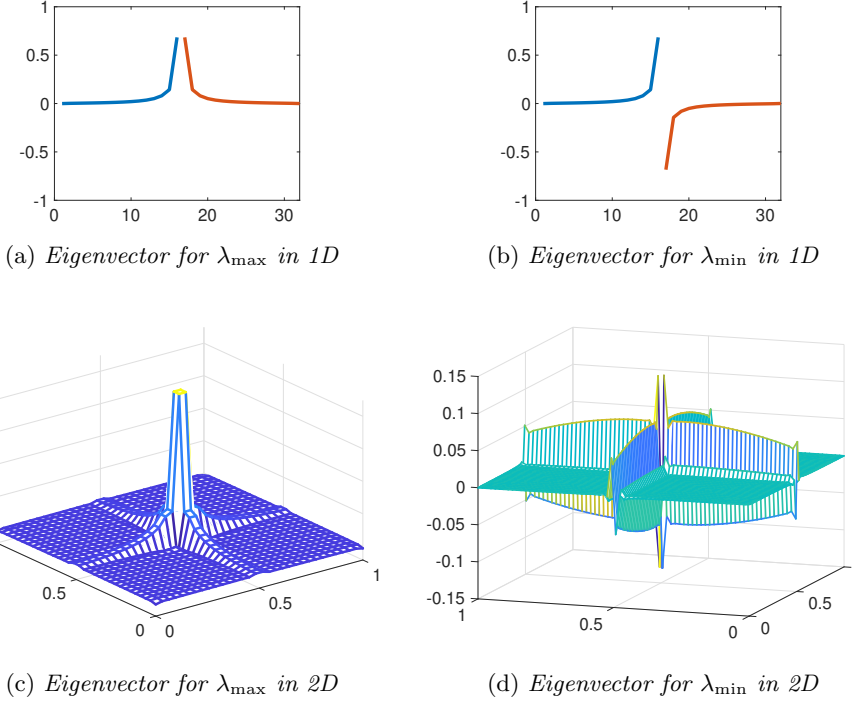


Fig. 5: Eigenvectors of $T_{\text{Jacobi}}^{-1}A$ in 1D ($N = 32, D = 2$) and 2D ($N = 32^2, D = 2^2$). The discretized integral operator is given in (2.4).

where λ is an eigenvalue. Write $x = x_1 + x_2$, where $x_i = R_i x$ for $i = 1, 2$. We state the following theorem and give the proof in [Appendix A](#).

THEOREM 3.7. *Let $x = x_1 + x_2$ be an eigenvector associated with an eigenvalue λ of the preconditioned matrix $T_{\text{Jacobi}}^{-1}A$ in 1D. Then, $x' = x_1 - x_2$ is also an eigenvector, and the corresponding eigenvalue is $2 - \lambda$. In other words,*

$$T_{\text{Jacobi}}^{-1}A x = \lambda x \Leftrightarrow T_{\text{Jacobi}}^{-1}A x' = (2 - \lambda) x'.$$

According to the above theorem, (3.5) implies

$$(3.8) \quad \lim_{N \rightarrow \infty} \lambda_{\min}(T_{\text{Jacobi}}^{-1}A) = 0$$

for our example in 1D; see numerical results of eigenvectors in [Figures 5a](#) and [5b](#). One interpretation of the eigenvectors of $T_{\text{Jacobi}}^{-1}A$ from electrostatics is the following. The limit ($N \rightarrow \infty$) of the eigenvector associated with λ_{\max} , namely, (3.6), can be interpreted as putting a point charge at the domain center. The eigenvector associated with λ_{\min} corresponds to putting dipoles near the boundaries of adjacent subdomains. For the example in 1D, the boundary is just one point $x_c = 1/2$; see [Figure 5b](#). For the unite square domain in 2D, the boundaries are two lines $1/2 \times [0, 1]$ and $[0, 1] \times 1/2$; see [Figure 5d](#). As a result, the electric potential induced by all charges cancels out approximately. Based on this intuition, we conjecture that (3.8) also holds when $d = 2$ and 3; see numerical results in [Table 3](#).

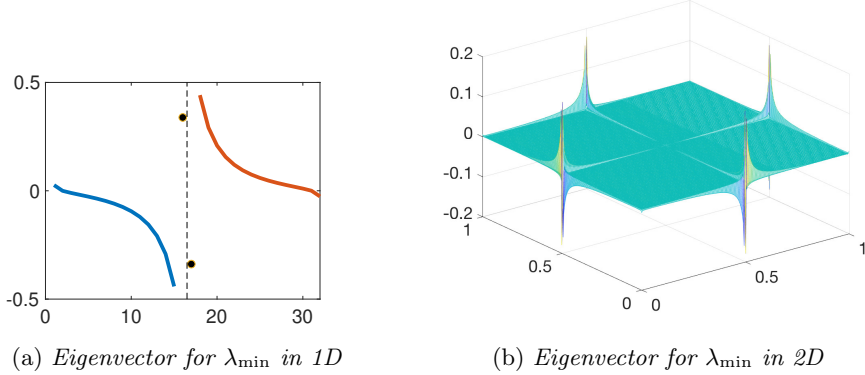


Fig. 6: Eigenvectors of $T_{\text{Schwarz}}^{-1} A$ in 1D ($N = 32, D = 2$) and 2D ($N = 256^2, D = 2^2$). In (a), two dots (in black) lie in the overlapped region of two subdomains, and two curves (in blue and red, respectively) lie in the interior of two subdomains, respectively. The discretized integral operator is given in (2.4).

Finally, we consider the minimum eigen-pair of $T_{\text{Schwarz}}^{-1} A$. Let us revisit the previous example in 1D, where the problem domain $\Omega = [0, 1]$ is discretized with a uniform grid of size N (an even integer) and the grid points are indexed from left to right. To construct the Schwarz preconditioner, we use the overlapping domain decomposition where Ω_1 and Ω_2 contain the first and the last $N/2 + 1$ grid points, respectively. Figure 6a shows the eigenvector corresponding to λ_{\min} . In the figure, there is a “dipole” at the overlapped region, and the eigenvector decays more slowly away from the boundary than that in Figure 5b. This observation extends to higher dimensions, and the differences between the two eigenvectors for λ_{\min} are more pronounced in 2D; compare Figure 6b to Figure 5d. Both eigenvectors contain “dipoles” near the boundaries of the four subdomains in 2D. For the eigenvector associated with the Schwarz preconditioner, the “dipoles” mainly concentrate around $(1/2, 0), (1/2, 1), (0, 1/2)$ and $(1, 1/2)$ on the boundary of the square domain. For the eigenvector associated with the block Jacobi preconditioner, however, the “dipoles” mainly exist in the interior of the domain. This empirical observation extends to cases when $D > 2^d$. The difference between the minimum eigenvalues of the preconditioned matrix is shown in Table 3 for problems in 2D and in 3D.

4. Coloring-based decomposition (CBD) and preconditioner. In this section, we introduce the CBD preconditioner based on the decomposition (2.9). Recall that a subdomain consists of spatially distant regions as shown in Figure 3d and the algebraic formulation of the CBD preconditioner is given in (3.2). In Section 4.1, we show that the maximum and minimum eigenvalues of the preconditioned matrix $T_{\text{CBD}}^{-1} A$ are bounded from above and from below, respectively. In Section 4.2, we apply the recursive skeletonization (RS) factorization [19] to construct approximate factorizations of subproblems in the CBD preconditioner, which are used to apply the preconditioner efficiently. In Section 4.3, we compare the CBD preconditioner to the original RS method, and in Section 4.4, we provide some analysis of the CBD preconditioner.

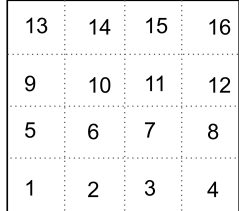
Table 3: Maximum and minimum eigenvalues of the preconditioned matrix (3.3). The block Jacobi, the Schwarz and the CBD preconditioners are defined in Table 1. The number of subdomains $D = 2^d$ is fixed.

N	D	Jacobi		Schwarz		CBD		
		λ_{\max}	λ_{\min}	λ_{\max}	λ_{\min}	M	λ_{\max}	λ_{\min}
8^2	4	2.8479	0.1695	4.0000	0.8209	2^2	4.0000	0.8209
16^2	4	3.1876	0.0838	4.0000	0.8237	4^2	4.0000	0.9201
32^2	4	3.3965	0.0419	4.0000	0.8280	8^2	4.0000	0.9397
64^2	4	3.5349	0.0210	4.0000	0.8305	16^2	4.0000	0.9403
128^2	4	3.6316	0.0105	4.0000	0.8317	32^2	4.0000	0.9399

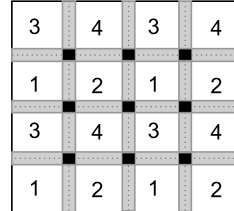
(a) Discretized integral operator in 2D; see (2.4).

N	D	Jacobi		Schwarz		CBD		
		λ_{\max}	λ_{\min}	λ_{\max}	λ_{\min}	M	λ_{\max}	λ_{\min}
4^3	8	4.0618	0.2602	8.0000	0.9750	2^3	8.0000	0.9750
8^3	8	4.6797	0.1532	8.0000	0.9408	4^3	8.0000	0.9965
16^3	8	5.1116	0.0850	8.0000	0.9020	8^3	8.0000	0.9992
32^3	8	5.4158	0.0451	8.0000	0.8661	16^3	8.0000	0.9998

(b) Discretized integral operator in 3D; see (2.5).



(a)



(b)

Fig. 7: (a) a square domain is partitioned uniformly into 16 partitions; (b) shared region (in black) of the four subdomains in the CBD preconditioner. Every subdomain has four separated regions indicated by the index.

4.1. Spectral equivalence. The number of subdomains used in the CBD preconditioner is typically a constant independent of the problem size. This implies that the maximum eigenvalue of the preconditioned matrix is upper bounded according to Theorem 3.1. In addition, numerical results reveal strong evidence that the minimum eigenvalue is lower bounded away from zero, which can also be justified by Conjecture 3.2. We illustrate these statements with more details in the following.

Consider the maximum eigenvalue of the preconditioned matrix $T_{\text{CBD}}^{-1}A$. As previously mentioned in section 2, we assume the problem domain $\Omega = [0, 1]^d$ is discretized with a uniform grid and is partitioned uniformly into $M = m^d$ partitions (m parti-

tions along every dimension); see [Figure 7a](#). In this case, we have $D = 2^d$ subdomains in the CBD preconditioner. There are $(m - 1)^d$ overlapped region shared by all subdomains; see [Figure 7b](#) for an example. When $M = D = 2^d$, the CBD preconditioner is reduced to the Schwarz preconditioner. We generalize the analysis in [Section 3.2](#) and [Theorem 3.6](#) to the following:

THEOREM 4.1. *Suppose the problem domain $\Omega = [0, 1]^d$ is partitioned uniformly. Given the overlapping decomposition in [\(2.9\)](#), where $M = m^d \geq D$, we have*

$$\lambda_{\max}(T_{\text{CBD}}^{-1}A) = 2^d,$$

and the corresponding eigen-space is of dimension $(2(m - 1))^d$ and consists of vectors that are nonzero only in the overlapped region shared by all 2^d subdomains.

Proof. The proof is almost identical to that of [Theorem 3.6](#), except there are $(m - 1)^d$ overlapped region shared by all subdomains. (Recall that every shared region has 2^d discretization points; see [Figure 4a](#).) \square

Next, we consider the minimum eigenvalue of the preconditioned matrix in [\(3.3\)](#). Assume we are given a partitioning of the problem domain as in [\(2.6\)](#), where the number of partitions $M = \mathcal{O}(N)$. We can construct the Schwarz and the CBD preconditioners based on [\(2.7\)](#) and [\(2.9\)](#), respectively. In this case, a subdomain in the CBD preconditioner is a union of non-adjacent subdomains in the Schwarz preconditioner. This implies that every subproblem solved in the Schwarz preconditioner is a diagonal block in a subproblem solved in the CBD preconditioner. As a concrete example, we have $\Omega_1^{\text{CBD}} = \Omega_1^{\text{Schwarz}} \cup \Omega_3^{\text{Schwarz}} \cup \Omega_9^{\text{Schwarz}} \cup \Omega_{11}^{\text{Schwarz}}$ in [Figure 7](#). Correspondingly, we know the discretization points satisfy the same relationship, i.e., $\mathcal{I}_1^{\text{CBD}} = \mathcal{I}_1^{\text{Schwarz}} \cup \mathcal{I}_3^{\text{Schwarz}} \cup \mathcal{I}_9^{\text{Schwarz}} \cup \mathcal{I}_{11}^{\text{Schwarz}}$. According to the definition [\(3.1\)](#), we have

$$A_1^{\text{CBD}} = \begin{bmatrix} A_1^{\text{Schwarz}} & \times & \times & \times \\ \times & A_3^{\text{Schwarz}} & \times & \times \\ \times & \times & A_9^{\text{Schwarz}} & \times \\ \times & \times & \times & A_{11}^{\text{Schwarz}} \end{bmatrix},$$

where \times stands for entries in the original matrix A but not in any A_i^{Schwarz} . In general, the CBD preconditioner uses (much) more entries in the original problem A than the related Schwarz preconditioner. A subproblem A_i^{CBD} contains $\mathcal{O}(N/2^d)$ entries in A , whereas a subproblem A_i^{Schwarz} contains only $\mathcal{O}(1)$ entries. Therefore, we expect the CBD preconditioner to be a better preconditioner. Compare $\lambda_{\min}(T_{\text{CBD}}^{-1}A)$ in [Table 3](#) to $\lambda_{\min}(T_{\text{Schwarz}}^{-1}A)$ in [Table 2](#). We state the following:

Conjecture 4.2. Let A be the discretized integral operator in [\(2.4\)](#) or [\(2.5\)](#). Given the overlapping domain decomposition [\(2.9\)](#), the CBD preconditioner T_{CBD}^{-1} is defined in [\(3.2\)](#). Then,

$$\lambda_{\min}(T_{\text{CBD}}^{-1}A) \geq C > 0,$$

where C is a positive constant.

4.2. Recursive skeletonization (RS) as subdomain solver. To construct the CBD preconditioner, we apply the RS algorithm to compute an approximate factorization of every subproblem A_i in the CBD preconditioner. The resulting factorizations consist of block triangular factors, which can be inverted easily for applying

the preconditioner. Suppose the subproblem A_i is associated with the subdomain

$$(4.1) \quad \Omega_i = \bigcup_{k=1}^{\tilde{M}} \tilde{\mathcal{P}}_k,$$

where $\tilde{M} = M/D = M/2^d$, and $\tilde{\mathcal{P}}_k$'s are spatially distant regions of the same color; see an example in [Figure 7b](#). To simplify notations, we drop the subscript i in A_i for the rest of this section, and we refer interested readers to [\[19\]](#) for more details.

Without loss of generality, write

$$(4.2) \quad A = \begin{pmatrix} A_{pp} & A_{pq} \\ A_{qp} & A_{qq} \end{pmatrix},$$

where rows/columns indices p and q correspond to $\tilde{\mathcal{P}}_1$ and the union of remaining regions in [\(4.1\)](#), respectively. Assume A_{qp} is numerically low-rank, we compute the following interpolative decomposition (ID) [\[9\]](#) :

$$(4.3) \quad A_{qp} = \begin{pmatrix} A_{qr} & A_{qs} \end{pmatrix} \approx A_{qs} \begin{pmatrix} T_p & I \end{pmatrix},$$

where the index set p is split into a *redundant* subset r and a *skeleton* subset s (up to a permutation) and

$$(4.4) \quad \|A_{qr} - A_{qs}T\| \leq \varepsilon \|A_{qr}\|$$

for a prescribed (relative) accuracy ε . We call the indices in s skeletons, which tend to be discretization points close to the boundary of $\tilde{\mathcal{P}}_1$. See a pictorial illustration in [Figure 8](#). Define the numerical rank $k = |s|$. Since $\tilde{\mathcal{P}}_1$ is well-separated from the remaining regions in [\(4.1\)](#), we know

$$(4.5) \quad k = \mathcal{O}(1),$$

according to standard fast multipole estimates [\[16, 17\]](#). Computing the ID requires $\mathcal{O}(k|p||q|)$ operations in general but can be accelerated to $\mathcal{O}(k|p|^2)$ operations using the so-called proxy trick [\[21, 39\]](#).

With [\(4.3\)](#), we have the approximation

$$A \approx \begin{pmatrix} A_{rr} & A_{rs} & T_p^\top A_{sq} \\ A_{sr} & A_{ss} & A_{sq} \\ A_{qs}T_p & A_{qs} & A_{qq} \end{pmatrix},$$

so we can eliminate the original A_{rq} and A_{qr} blocks without affecting the A_{qq} block:

$$(4.6) \quad L_p^\top A L_p \approx \begin{pmatrix} B_{rr} & B_{rs} \\ B_{sr} & A_{ss} & A_{sq} \\ A_{qs} & A_{qq} \end{pmatrix}, \quad L_p = \begin{pmatrix} I & & \\ -T_p & I & \\ & & I \end{pmatrix}$$

where

$$\begin{aligned} B_{rr} &= A_{rr} - A_{rs}T_p - T_p^\top A_{sr} + T_p^\top A_{ss}T_p, \\ B_{sr} &= B_{rs}^\top = A_{sr} - A_{ss}T_p. \end{aligned}$$

Let $B_{rr} = G_r^\top G_r$ be its Cholesky factorization, and we have the following approximate partial factorization

$$(4.7) \quad U_r^\top L_p^\top A L_p U_r \approx \begin{pmatrix} I & & \\ & B_{ss} & A_{sq} \\ & A_{qs} & A_{qq} \end{pmatrix}, \quad U_r = \begin{pmatrix} G_r^{-1} & -B_{rr}^{-1} B_{rs} \\ & I \\ & & I \end{pmatrix},$$

where

$$(4.8) \quad B_{ss} = A_{ss} - B_{sr} B_{rr}^{-1} B_{rs}.$$

Notice that the A_{qq} , A_{sq} , and A_{qs} blocks have not been modified. Define $R_1 = L_p U_r$ corresponding to the first region $\tilde{\mathcal{P}}_1$ in (4.1), and we call R_1 an “compress-then-eliminate” operator.

We continue the above “compress-then-eliminate” step for the remaining block rows/columns corresponding to each of the remaining regions in (4.1). The resulting Schur complement is a block matrix, where off-diagonal blocks remain sub-matrices in A . To be precise, suppose the indices of every block row/column are split into a redundant subset r_i and a skeleton subset s_i for $i = 1, 2, \dots, \tilde{M}$, then there exists a permutation matrix Q such that

$$(4.9) \quad Q^\top (R_{\tilde{M}}^\top \dots R_2^\top R_1^\top A R_1 R_2 \dots R_{\tilde{M}}) Q \approx \begin{pmatrix} I & & & \\ & B_{s_1 s_1} & A_{s_1 s_2} & \dots & A_{s_1 s_{\tilde{M}}} \\ & A_{s_2 s_1} & B_{s_2 s_2} & \dots & A_{s_2 s_{\tilde{M}}} \\ & \vdots & \vdots & & \vdots \\ & A_{s_{\tilde{M}} s_1} & A_{s_{\tilde{M}} s_2} & \dots & B_{s_{\tilde{M}} s_{\tilde{M}}} \end{pmatrix},$$

where the first diagonal block has size $\sum r_i$, and every $B_{s_i s_i}$ is computed analogously to (4.8). Figure 8 shows a pictorial illustration of the row/column indices in the original subproblem A_i and the Schur complement in (4.9).

To continue factorizing the Schur complement (approximately), we need a coarse partitioning of the domain Ω_i . It can be obtained by merging spatially close regions in (4.1). With a coarse overlapping domain, we repeat the above process recursively until only one coarse partition remains. As the last step, we factorize the remaining Schur complement with Cholesky factorization directly. In practice, we compute a hierarchical partitioning of the problem domain Ω , where the decomposition (4.1) is at the first level and the last Schur complement factorized with Cholesky factorization is at the last level. For convenience, we make the following definition:

DEFINITION 4.3. *The degrees of freedom (DOFs) at every level in a hierarchical partitioning of the problem domain Ω are the discretization points that have not been processed in the RS algorithm. In particular, we have*

- *DOFs at the first level: discretization points corresponding to A in (4.2);*
- *DOFs at the second level: discretization points corresponding to the Schur complement in (4.9);*
- *DOFs at the last level: discretization points corresponding to the last Schur complement factorized with Cholesky factorization.*

Assume in (4.3) the numerical rank $|s_i| \equiv k$ is a constant for all i . The number of DOFs at the second level is

$$(4.10) \quad \sum_{i=1}^{\tilde{M}} s_i = k\tilde{M},$$

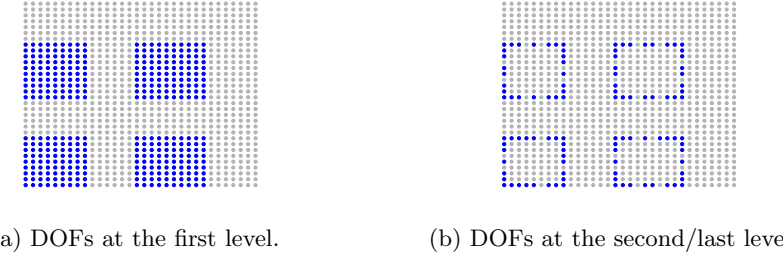


Fig. 8: *Illustration of applying the RS to a subproblem in the CBD preconditioner ($N = 32^2$, $M = 4^2$, and $\varepsilon = 10^{-6}$ in ID).*

which immediately leads to the following:

THEOREM 4.4. *In the CBD preconditioner, the number of DOFs at the second level is $\mathcal{O}(M)$, independent of the original problem size N .*

Recall that $M = D\tilde{M} = 2^d\tilde{M}$ is the number of partitions of the entire domain Ω . Here, we do not require $M = \mathcal{O}(N)$ as in Section 3. In fact, we show how to choose M to achieve optimal asymptotic scaling in Section 4.4.

4.3. Comparison to the original RS factorization. The original RS factorization was applied to matrix A in (1.2) directly, as other FDS's are typically used. To that end, the algorithm described in Section 4.2 remains the same except that we replace (4.1) with a partitioning (non-overlapping decomposition) of the entire problem domain as follows

$$(4.11) \quad \Omega = \bigcup_{i=1}^M \mathcal{P}_i, \quad \mathcal{P}_i \cap \mathcal{P}_j = \emptyset, \text{ if } i \neq j.$$

In particular, we view matrix A as a block matrix as in (4.2), where p and q correspond to \mathcal{P}_1 and $\bigcup_{i=2}^M \mathcal{P}_i$, respectively. Then, we compute the ID of A_{qp} as in (4.3). Since \mathcal{P}_1 is spatially adjacent to $\bigcup_{i=2}^M \mathcal{P}_i$, we know the following according to Green's theorem:

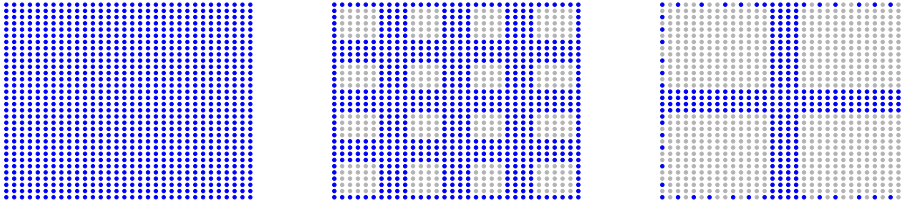
$$(4.12) \quad k = \mathcal{O}\left((N/M)^{\frac{d-1}{d}}\right).$$

With a uniform partitioning, \mathcal{P}_1 contains N/M discretization points, and the numerical rank k scales as the perimeter or the surface area of \mathcal{P}_1 in 2D or 3D, respectively. Compare (4.12) to the numerical rank in (4.5) corresponding to applying the RS to a subproblem A_i in the CBD preconditioner.

After A_{qp} is compressed, we follow (4.6) and (4.7), and we repeat the “compress-then-eliminate” step for each of the remaining block rows/columns and obtain the Schur complement as in (4.9). Assuming the numerical rank k is a constant for all blocks, the resulting Schur complement has size kM . To factorize the Schur complement, we construct a coarse partitioning of Ω by merging adjacent partitions in (4.11) and recurse until a single partition is left. Finally, we apply Cholesky factorization to the last Schur complement directly. Figure 9 shows a pictorial illustration of the entire algorithm.

Let S be the number of DOFs at the last level, and we have the following [19]:

$$(4.13) \quad S = \mathcal{O}\left(N^{(d-1)/d}\right).$$



(a) DOFs at the first level. (b) DOFs at the second level. (c) DOFs at the last level.

Fig. 9: *Illustration of applying RS to A ($N = 32^2$, $M = 4^2$, and $\varepsilon = 10^{-6}$ in ID).*

Since work required to factorize the last Schur complement typically dominates that of the RS algorithm, we have the following [19]:

THEOREM 4.5. *The construction cost of applying the RS algorithm to A in (1.2) is*

$$t_f = \mathcal{O}(N^{3(d-1)/d})$$

for $d = 2, 3$, and storing/applying the approximate factorization requires

$$m_f = t_a = \begin{cases} \mathcal{O}(N \log N), & d = 2, \\ \mathcal{O}(N^{4/3}), & d = 3. \end{cases}$$

Next, we derive results analogous to (4.13) and Theorem 4.5 for the CBD preconditioner. According to Theorem 4.4, the number of DOFs at the second level is $\mathcal{O}(M)$ in the CBD preconditioner. The DOFs corresponds to the Schur complement in (4.9), to which we apply the RS algorithm recursively. If we apply (4.13) to the Schur complement of size $\mathcal{O}(M)$, it is easy to see the following:

THEOREM 4.6. *In the CBC preconditioner, the number of DOFs at the last level is (upper bounded by)*

$$S = \mathcal{O}(M^{(d-1)/d}).$$

To construct the CBD preconditioner, we apply the RS algorithm to every subproblem A_i for $i = 1, 2, \dots, 2^d$. In general, suppose we have an FDS with CN^α construction cost, where C is a constant. Then, we immediately have

THEOREM 4.7. *The construction cost of the CBD preconditioner is*

$$2^d \cdot \tilde{C} \left(\frac{N}{2^d} \right)^\alpha = \frac{\tilde{C}}{C \cdot 2^{(\alpha-1)d}} CN^\alpha < CN^\alpha,$$

where $d = 2$ or 3 , $\tilde{C} < C$, and $\alpha > 1$. In particular, $\alpha = 3(d-1)/d$ for the RS factorization.

Here, the fact that $\tilde{C} < C$ comes from the decrease of off-diagonal rank from (4.12) to (4.5). To summarize, Table 4 shows the key differences between the original RS algorithm and the CBD preconditioner.

Remark 4.8. We can fix $D = 2^d$ and employ an FDS as the subdomain solver in the Schwarz preconditioner. Following the analysis above, it is obvious that the associated construct cost is $CN^\alpha/2^{(\alpha-1)d}$. In other words, the cost is higher by a factor of C/\tilde{C} than that of the CBD preconditioner.

Table 4: Comparison between the original RS factorization [19] (applied to A directly) and the CBD preconditioner (employing RS for every subproblem A_i).

	RS	CBD
Off-diagonal rank at first level	(4.12)	(4.5)
# DOFs at last level	(4.13)	Theorem 4.6
Construction cost	Theorem 4.5	Theorem 4.7

4.4. Asymptotically faster algorithm. Unlike that in the RS method, the number of DOFs at the last level in the CBD preconditioner depends on only the number of partitions M according to Theorem 4.6. In this section, we show that we can scale M sublinearly to the problem size N , and the construction of the CBD preconditioner becomes asymptotically faster. This approach, however, may be difficult to realize in practice and is *not* implemented.

Let us revisit the construction of the CBD preconditioner. In particular, we decompose the factorization cost into two terms: one for the first level and the other for all remaining levels. As previously mentioned, we apply the “compress-then-eliminate” step for $\mathcal{O}(M)$ times at the first level, where computing an ID and the subsequent elimination both require $\mathcal{O}((N/M)^3)$. If we plug in the asymptotic complexities of the RS in Theorem 4.5 for the $\mathcal{O}(M)$ DOFs at the second level, we obtain the following:

THEOREM 4.9. *Suppose we apply the RS solver to every subdomain in the CBD preconditioner. Define $P \equiv \mathcal{O}(N/M)$. The following complexities holds:*

(4.14)

$$t_f = \mathcal{O}(P^3 M + M^{3(d-1)/d}), \quad m_f = t_a = \begin{cases} \mathcal{O}(P^2 M + M \log M), & d = 2 \\ \mathcal{O}(P^2 M + M^{4/3}), & d = 3 \end{cases}$$

We note that the number of partitions M is a parameter in (4.14), so we can optimize the complexities to obtain asymptotically more efficient methods than the RS solver as the following corollary shows:

COROLLARY 4.10. *In 2D, let $M = \mathcal{O}(N^{6/7})$, and we have*

$$t_f = \mathcal{O}(N^{9/7}), \quad m_f = t_a = \mathcal{O}(N^{8/7}).$$

In 3D, let $M = \mathcal{O}(N^{3/4})$, and we have

$$t_f = \mathcal{O}(N^{3/2}), \quad m_f = t_a = \mathcal{O}(N^{5/4}),$$

Similarly, we can optimize the memory m_f (or equivalently t_a) in (4.14) with respect to M . In general, suppose we have an FDS of work complexity $\mathcal{O}(N^\alpha)$. Corollary 4.10 can be generalized to the following:

THEOREM 4.11. *Suppose we have an FDS with construction cost $\mathcal{O}(N^\alpha)$ when applied to A in (1.2). The optimal complexity to construct the CBD preconditioner employing the FDS as a subdomain solver is*

$$\min_M \mathcal{O}(P^3 M + M^\alpha) = \mathcal{O}(N^{3\alpha/(2+\alpha)}) < \mathcal{O}(N^\alpha),$$

where the minimum is obtained when $M = N^{3/(\alpha+2)}$.

5. Numerical results. In this section, we benchmark the CBD preconditioner and compare it to the RS factorization [19] on problems in 2D and in 3D. Recall the problem and the domain decompositions in Section 2. The RS solver was applied to solve the global problem (1.2) directly, while the CBD preconditioner employed the RS solver for every subdomain (4 and 8 subdomains in 2D and in 3D, respectively). We fixed $\varepsilon = 1e-3$ in (4.4) as the relative accuracy of low-rank approximations computed with the ID¹. We used the PCG to solve (1.2), where the matrix-vector (matvec) product with A was carried out via the fast Fourier transform (FFT). In the general case where the discretization grid is non-uniform, the FMM could be used for fast matvec. Below are the notations we used to report results of our experiments (timing and storage are in seconds and in GB, respectively):

- N : problem size/matrix size/number of discretization points;
- $M = \mathcal{O}(N)$: number of partitions of the problem domain in (2.6);
- S : number of DOFs at the last level in the RS solver and that associated with *one* subproblem in the CBD preconditioner (we report $2^d S$ over all subdomains for the CBD preconditioner);
- t_f : time of factorization to construct a preconditioner;
- m_f : storage of a preconditioner;
- t_s : time of applying a preconditioner;
- t_{pcg} : total PCG time for solving (1.2);
- n_{it} : number of PCG iterations to reach a relative residual of 10^{-12} .

All experiments were performed with MATLAB® R2020a on an Intel Xeon Platinum 8280M² (“Cascade Lake”) that has 2.1 TB of memory and 112 cores on four sockets (28 cores/socket). Results in Section 5.2 corresponding to solving problems in 2D were obtained using one thread, since intermediate matrices are relatively small that associated computation benefits little from multithreading. Results in Section 5.3 corresponding to solving problems in 3D were obtained using the default multithreading in MATLAB, where the maximum number of computational threads equals to the number of physical cores.

5.1. Exact CBD preconditioner. We show the number of PCG iterations with the exact CBD preconditioner, where subproblems are factorized with Cholesky factorization rather than the RS method. For comparison, we fixed the number of subdomains $D = 2^d$ in the Jacobi preconditioner and the Schwarz preconditioner to be the same as in the CBD preconditioner. Recall that the domain decomposition associated with the block Jacobi preconditioner is non-overlapping but those with the other two preconditioners are overlapping.

As Table 5 shows, the number of PCG iterations was almost constant with the two preconditioners based on overlapping domain decompositions. By contrast, the Jacobi preconditioner led to increasing PCG iterations as the problem size increased. All subproblems in the three preconditioners were factorized using Cholesky factorization, so the construction cost was $\mathcal{O}(N^3)$ for all preconditioners. As Remark 4.8 mentioned, we can apply an FDS to speedup the construction of the Schwarz preconditioner here, but it would not be as efficient as employing the FDS as a subdomain solver in the CBD preconditioner.

¹The radius of the proxy surface used to accelerate the computation of an ID was set to 1.5 as suggested in [19].

²<https://frontera-portal.tacc.utexas.edu/user-guide/system/#large-memory-nodes>

Table 5: *Number of PCG iterations n_{it} with the Jacobi preconditioner, the Schwarz preconditioner and the CBD preconditioner (without low-rank compression) in 2D (left) and in 3D (right). The number of partitions $M = D = 2^d$ is fixed for the block Jacobi and the Schwarz preconditioners. For the CBD preconditioner, we used $M = N/16$ and $M = N/8$ in 2D and in 3D, respectively.*

N	D	Jacobi	Schwarz	CBD	N	D	Jacobi	Schwarz	CBD
16^2	4	34	18	18	8^3	8	33	26	27
32^2	4	50	19	19	16^3	8	50	27	27
64^2	4	72	19	20	32^3	8	72	29	29
128^2	4	102	20	20					

Table 6: *2D results, where the problem size N is fixed and the number of non-overlapping partitions M varies. The matrix is defined in (2.4).*

N	M	S	t_f	m_f	t_s	n_{it}	t_{pcg}
256^2	16^2	1043	1.43e+1	1.37e-1	1.20e-1	7	1.17
256^2	32^2	1048	7.68	8.73e-2	1.30e-1	6	1.07
256^2	64^2	1048	8.62	7.98e-2	3.04e-1	6	2.19
256^2	128^2	1047	1.20e+1	7.98e-2	9.40e-1	6	5.94

(a) *RS preconditioner based on the domain partitioning (2.6).*

N	M	$4S$	t_f	m_f	t_s	n_{it}	t_{pcg}
256^2	8^2	256	4.76	3.39e-1	1.73e-1	26	5.71
256^2	16^2	456	2.08	1.13e-1	8.18e-2	26	3.10
256^2	32^2	851	1.84	5.53e-2	1.07e-1	24	3.76
256^2	64^2	1627	5.20	6.86e-2	3.27e-1	22	8.47

(b) *CBD preconditioner based on the overlapping domain decomposition (2.9) (four subdomains).*

5.2. Two dimensions. The RS method is based on domain partitioning (2.6), where the number of partitions M is a parameter. The CBD preconditioner is based on overlapping domain decomposition (2.9), where the number of partitions is also a parameter to be chosen. Tables 6a and 6b show results of experiments with a fixed problem size but different numbers of partitions. Observe that S , the number of DOFs at the last level, is almost a constant for the RS method ((4.13)), whereas $S = \mathcal{O}(M^{1/2})$ for the CBD preconditioner (Theorem 4.6). Results in Tables 6a and 6b also indicate appropriate M for the two methods. In Table 6a, results are similar between $M = 32^2$ and $M = 64^2$; so we chose $N/M = 64$ in the RS solver for large problem sizes as done in [19, 24]. In Table 6b, $M = 32^2$ led to half of the factorization time and the memory footprint than $M = 16^2$; so we also chose $N/M = 64$ in the CBD preconditioner.

Table 7a shows results for solving large problem sizes with the RS method, where the factorization time was always an order of magnitude larger than the PCG time.

Table 7: 2D results, where the problem size per partition, i.e., N/M , is fixed. The matrix is defined in (2.4).

N	M	S	t_f	m_f	t_s	n_{it}	t_{pcg}
512^2	64^2	2072	5.64e+1	4.25e-1	4.42e-1	7	4.22
1024^2	128^2	4112	4.57e+2	2.01	1.84	8	2.01e+1
2048^2	256^2	5713	1.67e+3	7.32	7.40	15	1.34e+2
4096^2	512^2	8897	8.05e+3	2.88e+1	3.17e+1	19	8.22e+2
8192^2	1024^2	15303	3.88e+4	1.05e+2	1.51e+2	27	5.44e+3
16384^2	-	-	-	-	-	-	-

(a) RS preconditioner based on the domain partitioning (2.6).

N	M	$4S$	t_f	m_f	t_s	n_{it}	t_{pcg}
1024^2	128^2	2269	3.55e+1	9.09e-1	1.77	25	5.97e+1
2048^2	256^2	4207	1.56e+2	3.64	7.34	25	2.31e+2
4096^2	512^2	8263	7.99e+2	1.48e+1	3.58e+1	25*	1.27e+3
8192^2	1024^2	16433	3.91e+3	5.92e+1	1.80e+2	31*	7.52e+3
16384^2	2048^2	27034	2.03e+4	2.37e+2	8.94e+2	28*	3.49e+4

(b) CBD preconditioner based on the overlapping domain decomposition (2.9) (four subdomains). *PCG stagnated at relative residuals $1.13e-12$, $1.71e-12$, and $3.99e-12$, respectively.

Due to an increasing condition number of the discretized integral operator defined in (2.4), we observe that S increased slower than the predicted $\mathcal{O}(N^{1/2})$ scaling; the factorization time t_f scaled slower than the predicted $\mathcal{O}(N^{3/2})$ scaling, and the number of PCG iterations n_{it} increased. (This phenomenon is known in [19]; see Table 5.3, 3rd row when $\varepsilon = 1e-3$.) The expected behaviors such as $S = \mathcal{O}(N^{1/2})$ can be obtained by employing larger ranks in (4.3) through either decreasing ε in (4.4) or reducing the radius of the proxy surface. Both require extra computation and would lead to longer factorization time.

To compare with the RS solver, Table 7b shows corresponding results of the CBD preconditioner, where the factorization time and the PCG time are well balanced. The factorization time t_f of the CBD preconditioner was an order of magnitude smaller than that of the RS solver. In addition, the storage m_f of the CBD preconditioner was approximately half of that required by the RS solver. As expected, the CBD preconditioner led to more PCG iterations than the RS solver, but every PCG iteration took about the same amount of time with both methods. Overall, the total running time with the CBD preconditioner was approximately a quarter of that with the RS solver.

In the CBD preconditioner, S , the number of DOFs at the last level, increased as $\mathcal{O}(N^{1/2})$ until N reached 16384^2 , indicating that the ill-conditioning effect associated with the RS solver was mitigated. However, ill-conditioning still affected the convergence with the CBD preconditioner, preventing the PCG from reaching the relative residual $1e-12$ when $N \geq 4096^2$. On a computer with 2.1 TB memory, we used the CBD preconditioner to solve problems as large as $N = 16,384^2 \approx 2.7 \times 10^8$, for which

Table 8: 3D results, where the problem size N is fixed and the number of non-overlapping partitions M varies. The matrix is defined in (2.5).

N	M	S	t_f	m_f	t_s	n_{it}	t_{pcg}
32^3	4^3	5987	1.33e+1	3.97e-1	1.54e-1	5	8.55e-1
32^3	8^3	5982	1.60e+1	3.77e-1	1.92e-1	5	1.04
32^3	16^3	5990	1.83e+1	3.78e-1	3.65e-1	5	1.91

(a) RS preconditioner based on the domain partitioning (2.6).

N	M	$8S$	t_f	m_f	t_s	n_{it}	t_{pcg}
32^3	4^3	4209	3.45	2.24e-1	1.22e-1	33	4.83
32^3	8^3	10862	1.01e+1	2.91e-1	1.53e-1	32	5.19
32^3	16^3	32954	6.17e+1	1.65	1.02	28	2.88e+1

(b) CBD preconditioner based on the overlapping domain decomposition (2.9) (eight subdomains).

Table 9: 3D results, where the problem size per partition, i.e., N/M , is fixed. The matrix is defined in (2.5).

N	M	S	t_f	m_f	t_s	n_{it}	t_{pcg}
32^3	4^3	5987	1.33e+1	3.97e-1	1.54e-1	5	8.55e-1
64^3	8^3	24081	4.32e+2	7.60	2.57	6	1.60e+1
128^3	16^3	97073	1.28e+4	1.40e+2	5.63e+1	7	3.99e+2
256^3	-	-	-	-	-	-	-

(a) RS preconditioner based on the domain partitioning (2.6).

N	M	$8S$	t_f	m_f	t_s	n_{it}	t_{pcg}
32^3	4^3	4209	3.31	2.24e-1	1.23e-1	33	4.44
64^3	8^3	9637	2.68e+1	2.15	1.25	35	4.54e+1
128^3	16^3	28476	2.60e+2	1.92e+1	1.13e+1	35	4.04e+2
256^3	32^3	87313	2.62e+3	1.65e+2	1.90e+2	35	6.77e+3

(b) CBD preconditioner based on the overlapping domain decomposition (2.9) (eight subdomains).

the original RS solver ran out of memory.

5.3. Three dimensions. As in Section 5.2, we first show results of experiments with a fixed problem size but different numbers of partitions in Tables 8a and 8b. Again, we observe results predicted by (4.13) and Theorem 4.6: S depends on M but not N in the CBD preconditioner, whereas S does not depend on M in the RS method. To solve large problems, we chose $N/M = 8^3 = 512$ for both methods according to

Tables 8a and **8b**. We remark that this choice for the RS method is different from that in [19] because we use multithreading and can handle large matrices more efficiently.

Table 9a shows results of the RS solver for large problem sizes, where the factorization time was at least two orders of magnitude larger than the PCG time. Observe that the numerical results basically match what (4.13) and **Theorem 4.5** predict: (1) $S = \mathcal{O}(N^{2/3})$; (2) $t_f = \mathcal{O}(N^2)$; and (3) $m_f = t_s = \mathcal{O}(N^{4/3})$. In addition, the number of PCG iterations n_{it} is almost constant. It is also clear from the table that the factorization time is prohibitive for a large problem size.

Table 9b shows results of the CBD preconditioner, which required much less factorization time and storage than the RS method. For example, compare the RS method to the CBD preconditioner when $N = 128^3$: (1) the factorization time of the CBD preconditioner was approximately two orders of magnitude smaller than that of the RS solver; (2) the storage of the CBD preconditioner was approximately one seventh of that used by the RS solver; and (3) both methods took approximately the same PCG time, although the CBD preconditioner required more iterations. Empirically, the factorization time and the storage of the CBD preconditioner both scaled closely to $\mathcal{O}(N)$. This indicates that the estimates in **Theorems 4.6** and **4.7** may be too pessimistic.

6. Conclusions. We introduce the CBD for constructing an overlapping domain decomposition, where the number of subdomains is independent of the problem size, and every subdomain consists of spatially distant regions. The associated CBD (single-level additive Schwarz) preconditioner led to $\mathcal{O}(1)$ PCG iterations for solving SPD linear systems, which arises from the discretization of first-kind Fredholm integral equations for Laplace's equation in 2D and 3D. We apply the RS factorization to construct the CBD preconditioner efficiently, and our numerical results show that the new preconditioner is much more efficient than the original RS method, especially for solving problems in 3D. Two future research directions include

- Incorporating other FDSs for subproblems in the CBD preconditioner. Some candidates include the HIF [19], the RS-S [24] and the IFMM [11], all of which have been shown to achieve quasi-linear complexities (under mild assumptions) for solving problems in both 2D and 3D.
- Extending our approach to solving SPD linear systems arising from machine learning and data science, where the coefficient matrix (a.k.a., kernel matrix) is generated by positive definite functions [33]. When the underlying data set lies in a low-dimensional space [32] or even in a high-dimensional space for some applications [8], the coefficient matrix also has the hierarchical low-rank structure we exploit.

Appendix A. Proof of **Theorem 3.7**.

Proof. Write $T_{\text{Jacobi}}^{-1}A = P_1 + P_2$, where P_i is defined in (3.4). Rewrite (3.7) as

$$(P_1 + P_2)(x_1 + x_2) = \lambda(x_1 + x_2)$$

Lemma 3.5 $\xrightarrow{} P_1x_2 + P_2x_1 = (\lambda - 1)(x_1 + x_2).$

Applying projections $R_1R_1^\top$ and $R_2R_2^\top$ on both sides, we obtain

$$(A.1) \quad \begin{cases} P_1x_2 = (\lambda - 1)x_1, \\ P_2x_1 = (\lambda - 1)x_2. \end{cases}$$

Therefore, we know that

$$\begin{aligned}
 (P_1 + P_2)(x_1 - x_2) &\stackrel{\text{Lemma 3.5}}{=} (x_1 - x_2) + P_2 x_1 - P_1 x_2 \\
 &\stackrel{(A.1)}{=} (x_1 - x_2) - (1 - \lambda)x_2 + (1 - \lambda)x_1 \\
 &= (2 - \lambda)(x_1 - x_2). \quad \square
 \end{aligned}$$

REFERENCES

- [1] A. AMINFAR, S. AMBIKASARAN, AND E. DARVE, *A fast block low-rank dense solver with applications to finite-element matrices*, Journal of Computational Physics, 304 (2016), pp. 170–188.
- [2] K. APPEL, W. HAKEN, AND J. KOCH, *Every planar map is four colorable. Part II: Reducibility*, Illinois Journal of Mathematics, 21 (1977), pp. 491–567.
- [3] C. BORGES AND G. BIROS, *A domain decomposition preconditioning for the integral equation formulation of the inverse scattering problem*, arXiv preprint arXiv:1901.09162, (2019).
- [4] T. F. CHAN, T. P. MATHEW, ET AL., *Domain decomposition algorithms*, Acta numerica, 3 (1994), pp. 61–143.
- [5] S. CHANDRASEKARAN, P. DEWILDE, M. GU, W. LYONS, AND T. PALS, *A fast solver for HSS representations via sparse matrices*, SIAM Journal on Matrix Analysis and Applications, 29 (2007), pp. 67–81.
- [6] S. CHANDRASEKARAN, M. GU, AND T. PALS, *A fast ULV decomposition solver for hierarchically semiseparable representations*, SIAM Journal on Matrix Analysis and Applications, 28 (2006), pp. 603–622.
- [7] C. CHEN, S. AUBRY, T. OPPELSTRUP, A. ARSENIS, AND E. DARVE, *Fast algorithms for evaluating the stress field of dislocation lines in anisotropic elastic media*, Modelling and Simulation in Materials Science and Engineering, 26 (2018), p. 045007.
- [8] C. CHEN, S. REIZ, C. D. YU, H.-J. BUNGARTZ, AND G. BIROS, *Fast approximation of the Gauss–Newton Hessian matrix for the multilayer perceptron*, SIAM Journal on Matrix Analysis and Applications, 42 (2021), pp. 165–184.
- [9] H. CHENG, Z. GIMBUTAS, P.-G. MARTINSSON, AND V. ROKHLIN, *On the compression of low rank matrices*, SIAM Journal on Scientific Computing, 26 (2005), pp. 1389–1404.
- [10] E. CORONA, P.-G. MARTINSSON, AND D. ZORIN, *An $O(N)$ direct solver for integral equations on the plane*, Applied and Computational Harmonic Analysis, 38 (2015), pp. 284–317.
- [11] P. COULIER, H. POURANSARI, AND E. DARVE, *The inverse fast multipole method: using a fast approximate direct solver as a preconditioner for dense linear systems*, SIAM Journal on Scientific Computing, 39 (2017), pp. A761–A796.
- [12] V. DOLEAN, P. JOLIVET, AND F. NATAF, *An introduction to domain decomposition methods: algorithms, theory, and parallel implementation*, SIAM, 2015.
- [13] W. FONG AND E. DARVE, *The black-box fast multipole method*, Journal of Computational Physics, 228 (2009), pp. 8712–8725.
- [14] A. GILLMAN, P. M. YOUNG, AND P.-G. MARTINSSON, *A direct solver with $O(N)$ complexity for integral equations on one-dimensional domains*, Frontiers of Mathematics in China, 7 (2012), pp. 217–247.
- [15] L. GREENGARD, D. GUEYFFIER, P.-G. MARTINSSON, AND V. ROKHLIN, *Fast direct solvers for integral equations in complex three-dimensional domains*, Acta Numerica, 18 (2009), pp. 243–275.
- [16] L. GREENGARD AND V. ROKHLIN, *A fast algorithm for particle simulations*, Journal of computational physics, 73 (1987), pp. 325–348.
- [17] L. GREENGARD AND V. ROKHLIN, *A new version of the fast multipole method for the Laplace equation in three dimensions*, tech. report, YALE UNIV NEW HAVEN CT DEPT OF COMPUTER SCIENCE, 1996.
- [18] K. L. HO AND L. GREENGARD, *A fast direct solver for structured linear systems by recursive skeletonization*, SIAM Journal on Scientific Computing, 34 (2012), pp. A2507–A2532.
- [19] K. L. HO AND L. YING, *Hierarchical interpolative factorization for elliptic operators: integral equations*, Comm. Pure Appl. Math, 69 (2016), pp. 1314–1353.
- [20] D. MALHOTRA AND G. BIROS, *PVFMM: A parallel kernel independent fMM for particle and volume potentials*, Communications in Computational Physics, 18 (2015), pp. 808–830.
- [21] P.-G. MARTINSSON, *Fast direct solvers for elliptic PDEs*, SIAM, 2019.

- [22] P.-G. MARTINSSON AND V. ROKHLIN, *A fast direct solver for boundary integral equations in two dimensions*, Journal of Computational Physics, 205 (2005), pp. 1–23.
- [23] P.-G. MARTINSSON AND V. ROKHLIN, *An accelerated kernel-independent fast multipole method in one dimension*, SIAM Journal on Scientific Computing, 29 (2007), pp. 1160–1178.
- [24] V. MINDEN, K. L. HO, A. DAMLE, AND L. YING, *A recursive skeletonization factorization based on strong admissibility*, Multiscale Modeling & Simulation, 15 (2017), pp. 768–796.
- [25] P. MUND, E. P. STEPHAN, AND J. WEISSE, *Two-level methods for the single layer potential in \mathbb{R}^3* , Computing, 60 (1998), pp. 243–266.
- [26] K. NABORS, S. KIM, AND J. WHITE, *Fast capacitance extraction of general three-dimensional structures*, IEEE transactions on microwave theory and techniques, 40 (1992), pp. 1496–1506.
- [27] K. NABORS, F. KORSMEYER, F. T. LEIGHTON, AND J. WHITE, *Preconditioned, adaptive, multipole-accelerated iterative methods for three-dimensional first-kind integral equations of potential theory*, SIAM Journal on Scientific Computing, 15 (1994), pp. 713–735.
- [28] B. QUAIFE AND G. BIROS, *On preconditioners for the Laplace double-layer in 2D*, Numerical Linear Algebra with Applications, 22 (2015), pp. 101–122.
- [29] J. R. SHEWCHUK ET AL., *An introduction to the conjugate gradient method without the agonizing pain*, 1994.
- [30] T. TAKAHASHI, C. CHEN, AND E. DARVE, *Parallelization of the inverse fast multipole method with an application to boundary element method*, Computer Physics Communications, 247 (2020), p. 106975.
- [31] T. TRAN, *Overlapping additive Schwarz preconditioners for boundary element methods*, The Journal of Integral Equations and Applications, (2000), pp. 177–207.
- [32] R. WANG, C. CHEN, J. LEE, AND E. DARVE, *PBBFMM3D: a parallel black-box algorithm for kernel matrix-vector multiplication*, Journal of Parallel and Distributed Computing, 154 (2021), pp. 64–73.
- [33] H. WENDLAND, *Scattered data approximation*, vol. 17, Cambridge university press, 2004.
- [34] J. XIA, *Robust and effective eSIF preconditioning for general SPD matrices*, arXiv preprint arXiv:2007.03729, (2020).
- [35] J. XIA, *Multi-layer hierarchical structures*, CSIAM Transaction of Applied Mathematics, 2 (2021), pp. 263–296.
- [36] J. XIA, S. CHANDRASEKARAN, M. GU, AND X. S. LI, *Fast algorithms for hierarchically semiseparable matrices*, Numerical Linear Algebra with Applications, 17 (2010), pp. 953–976.
- [37] X. XING AND E. CHOW, *Preserving positive definiteness in hierarchically semiseparable matrix approximations*, SIAM Journal on Matrix Analysis and Applications, 39 (2018), pp. 829–855.
- [38] X. XING, H. HUANG, AND E. CHOW, *Efficient construction of an HSS preconditioner for symmetric positive definite H^2 matrices*, SIAM Journal on Matrix Analysis and Applications, 42 (2021), pp. 683–707.
- [39] L. YING, G. BIROS, AND D. ZORIN, *A kernel-independent adaptive fast multipole algorithm in two and three dimensions*, Journal of Computational Physics, 196 (2004), pp. 591–626.